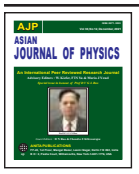

Asian Journal of Physics
Vol. 30, No 12 (2021) 1637-1646
Available on: www.asianjournalofphysics.com

ap

Wavelength dependent cubic nanoparticles formation on copper surfaces by femtosecond laser irradiation

Md Abu Taher, D Narayana Rao, and Sri Ram G Naraharisetty

School of Physics, University of Hyderabad, Hyderabad-500 046, India

This article is dedicated to Prof DVGLN Rao

The effect of changing the incident laser wavelength on the surface morphology is shown via femtosecond laser direct writing on a copper surface. For the first time in the literature, we demonstrated the formation of the cubic-shaped nanoparticles (NPs) on the laser-irradiated copper surface at the incident wavelength of 860 nm. We observed the formation of laser-induced periodic surface structures (LIPSS) are favorable over a broad range of laser fluences at 900 nm irradiation wavelength. We presented the variation of low spatial frequency LIPSS (LSFL) periodicity with the change of the fluence. We did not observe clear LIPSS formation at 960 nm irradiation on the copper surface out of the four wavelengths used. The energy dispersive X-ray (EDX) spectroscopic analysis on the cubic nanostructures reveals the presence of oxygen on the copper surface. The specific copper oxygen composite formation can be achieved at 860nm.

Keywords: Laser-induced periodic surface structures (LIPSS), Low spatial frequency LIPSS, Copper nanoparticles, Cubic-shaped nanoparticles, Laser direct Writing.

1 Introduction

The fabrication and investigation of metallic nanoparticles (NPs) gained tremendous attention from research communities due to their diverse applications in industry and academia [1-3]. These NPs can be used in energy storage and conservation devices [4-6], as catalytic materials [3,7], in environmental technology [7-10], biological sensing applications [11,12], surface-enhanced Raman scattering [13-15], and many more. The use of NPs for catalyst activity triggered the research for synthesis of functionalized NPs including graphene-based catalysts [16], nanocarbon-based catalysts [17], core/shell nano catalysts [18], magnetic supported nano catalysts [19,20], etc. These various needs have been justified by rapid synthesis and preparation of NPs of different-shapes, sizes, and morphologies using various methods such as solution-based preparation, e-beam lithography, extraction from the natural biological plants, and laser-induced NPs synthesis [21-25], etc. The fabrication of NPs using above mentioned conventional methods involve multiple steps, complexity, skill dependence and they are time-consuming. The fabrication of NPs by ultrafast laser irradiation offers a simple, one-step, and environmentally friendly method. It is a reliable technique of preparing NPs, because of its repeatability, controlled precise fabrication and pollution-free method [13,14,22,26].

Ultrafast laser ablation of metallic surfaces was reported using nanoseconds, picosecond, femtosecond pulsed lasers to fabricate superhydrophobic surfaces [27-30], antireflective surfaces [31-33], and various functional surfaces [30,34]. The underlying mechanisms of laser ablation depend on the materials used, irradiation parameters such as incident wavelength, pulse width, repetition rate, scanning speed or number of pulses per spot, and intensity of laser beams [35-39]. Most effective plasmonic NPs are gold and silver,

Corresponding author
e mail: *srgopal234@gmail.com* (N Sri Ram Gopal)

but their use in industrial puposes is limited due the associated cost. In this aspect the copper NPs got special attension due Due to its superior performance in terms of heat and electrical conductivity, catalytic activity, and cost-effectiveness [3,5].

Many researchers use femtosecond lasers for laser writing either at its fundamental frequency or at the second harmonic frequency. However, high-power lasers allow one to tune the frequencies continuously over a broad range with the help of optical parametric amplifiers. The effect of driving force frequency on the formation of the nanostructures and morphology is a relatively unexplored area of research. In this work, for the first time in the literature, we report the fabrication of laser-induced cubic shaped copper NPs decorating the laser structured surfaces. Also, we reported the formations of laser-induced periodic surface structures (LIPSS) with varying incident wavelengths. We observed that cubic-shaped copper NPs can be fabricated at only particular incident laser wavelength and at optimized laser parameters. The formation mechanism, properties of the nanoparticles, and LIPSS are discussed in this work.

2 Experimental procedure

We used Ti: Sapphire femtosecond laser pulses of 75 fs time duration, at repetition rate of 1 kHz, 800 nm central wavelength, and energy of 6 mJ per pulse. However, we used 3 mJ/pulse energy to pump commercially purchased optical parametric amplifier (TOPAS Prime, Light Conversion) to generate tunable wavelength of the laser beam from 300 nm - 2400 nm. After initial optimization, we chose to report four wavelengths, viz.: 800 nm, 860 nm, 900 nm, and 960 nm, to irradiate the copper substrate. A microscopic objective of 10X with a numerical aperture of 0.25 is used to focus the laser beam on the substrate's surface, as shown in Fig 1. The substrates were moved on raster scanning with the help of the 3D Newport nano-positioner stage, which is controlled by the ESP motion controller. The substrates were moved with a fixed scanning speed of 0.2 mm/s, and 100 µm spacing was maintained between the successive scanning. The surface morphologies are characterized by Field Emission Scanning Electron Microscope (FESEM, Zeiss Ultra55).

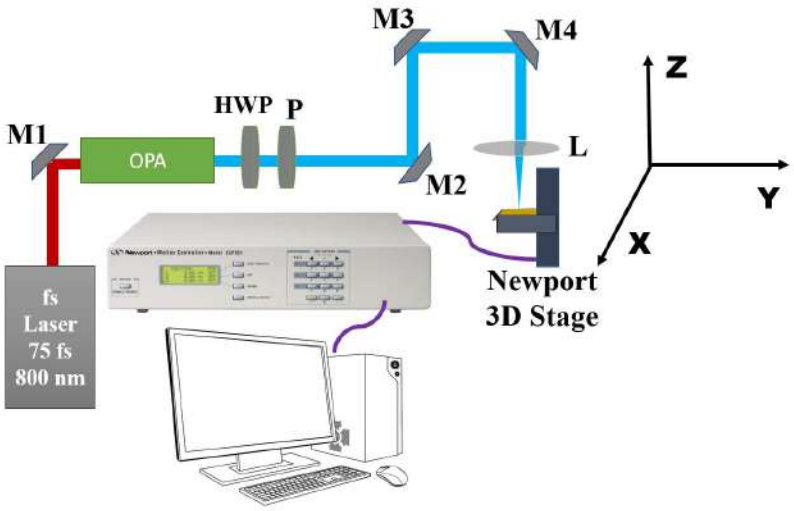

Fig 1. Schematics of laser direct writing set-up.

3 Results and discussions

Our initial goal is to study the variation of the LIPSS spatial periodicity over a broad range of incident wavelengths from 400 nm to 2000 nm on different materials. While working on copper surfaces, only at

particular wavelengths, we found unique nano-shaped surface features as serendipity. In this work, we report only that narrow range of incident wavelengths, where special structures are forming. The femtosecond laser beam is focused with microscopic objectives (10X/0.25) on copper substrates with four incident wavelengths viz.: 800, 860, 900, and 960 nm, at a fixed scanning speed of 0.2 mm/s. The incident laser fluences for each wavelength are presented in Table 1.

Table 1. Laser fluences for each wavelength at which the laser direct writing experiments were performed on the copper substrates

Fluence (J/cm^2)			
800 nm	860 nm	900 nm	960 nm
2.5	3.1	2.7	1.3
4.1	3.9	3.5	2.4
4.9	4.1	3.9	2.9
5.4	7.1	6.7	3.7

3.1. Surface morphology

3.1.1. Laser direct writing at 800 nm

Different surface topographical structures of laser-induced copper surfaces are shown in Fig 2. On each image, the incident fluence used is indicated on the left top corner, and all are irradiated with a fixed central wavelength of 800 nm (Fig 2). The low spatial frequency LIPSS (LSFL) are formed at fluence of 2.5 J/cm^2, and their spatial periodicity of LSFL is 515±14 nm. The magnified area of each surface is shown in the bottom row of (Fig 2). With the increment in fluence, LSFLs tend to get destroyed at the center of the focused beam and form feeble structures at the edges. As the fluence increases, LIPSS gets destroyed (LSFL) randomly distributed and irregularly shaped particles formation is observed.

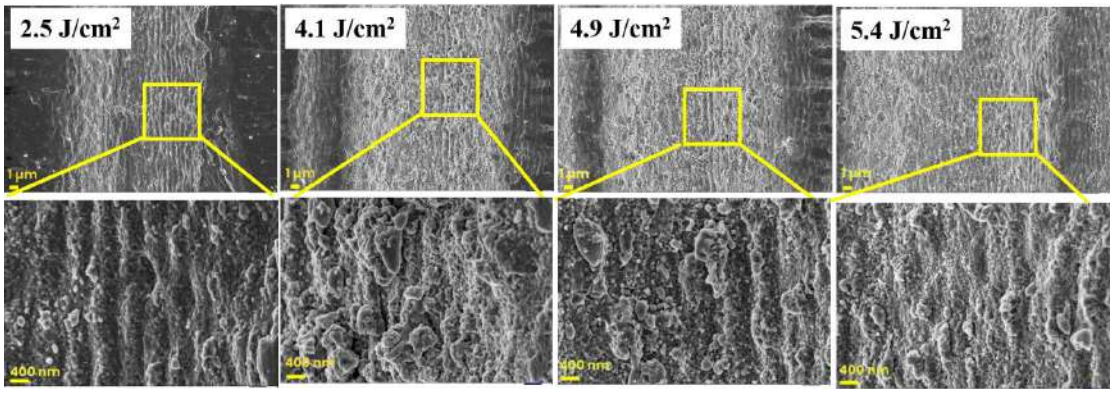

Fig 2. FESEM images of laser-induced copper surfaces for various fluences for the incident wavelength of 800 nm. The scanning speed is fixed at 0.2 mm/s. Scale bars are equal to 1 µm and 400 nm of the images in the first and second rows, respectively.

3.1.2. Laser direct writing at the central wavelength of 860 nm

Figure 3 represents the surface morphology of laser irradiated surfaces with the incident wavelength 860 nm. The fluence varies from 3.1 to 7.1 J/cm^2 with a constant scanning speed of 0.2 mm/s. At this incident wavelength, the response of the copper surface is significantly different in many aspects. There is the formation of LSFL with the spatial periodicity of 732±35 nm at the incident laser fluence of 4.1 J/cm^2. In the fluence range 3.1- 3.9 J/cm^2, the most notable interesting surface morphological features are appeared. Apart from the LSFL, we observe the formation of cubic-shaped copper nanoparticles of variable sizes. The

particle's average size is found to be 127 nm and 101 nm for the incident fluence of 3.1 J/cm^2 and 3.9 J/cm^2, respectively. It indicates that the particle size reduces as the fluence increases. On further increase in incident fluence, the formation of cubic-shaped particles is reduced and they are sparsely distributed over the LSFL ridges.

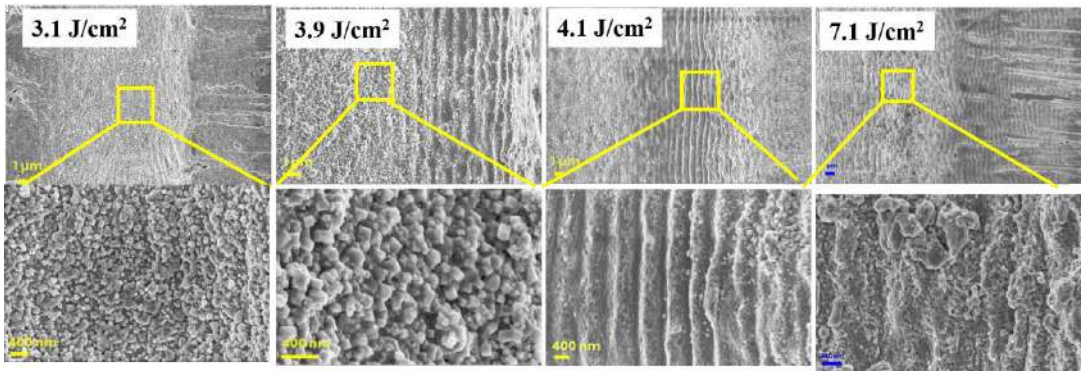

Fig 3. Surface morphologies of laser-induced copper surfaces at various laser fluences with the incident wavelength of 860 nm. The scanning speed is fixed at 0.2 mm/s. Scale bars are equal to 1 µm and 400 nm of the images in the first and second rows, respectively.

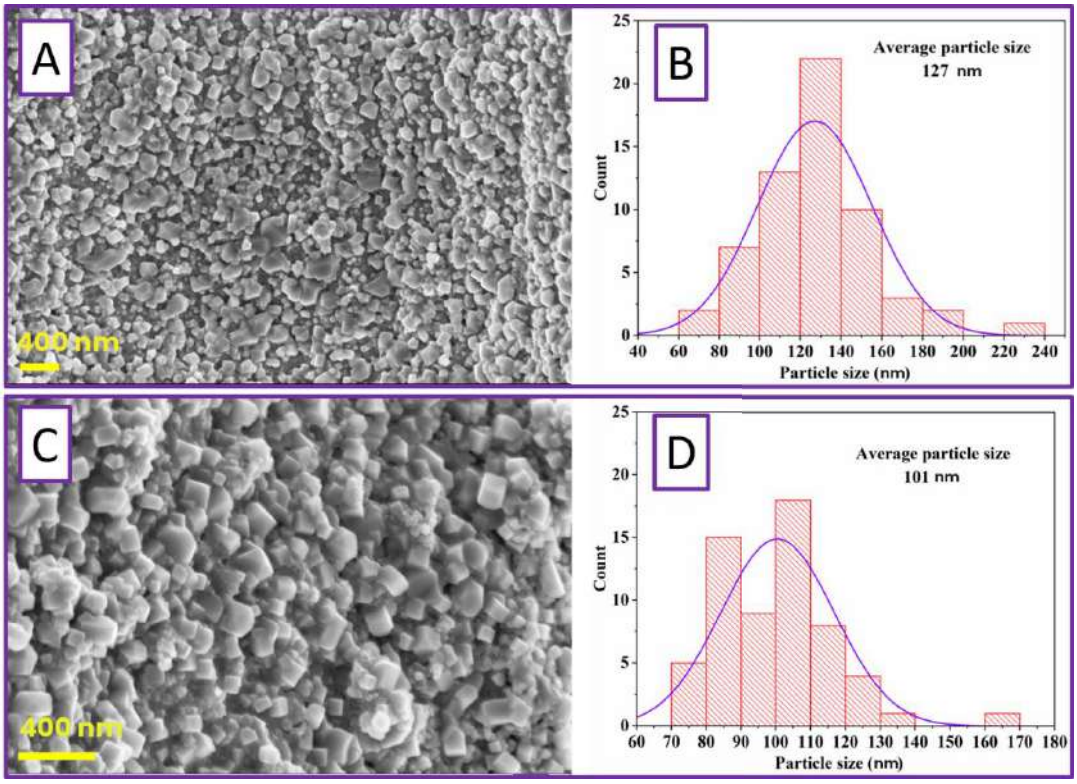

Fig 4. Distribution of copper NPs at the laser fluences of 3.1 J/cm^2 (A & B), and 3.9 J/cm^2 (C & D) on laser-irradiated copper surfaces at 860 nm incident wavelength.

Figure 4 depicts that the size of NPs change as the fluence increases; it also illustrates the impact on the shape of the copper nanoparticles. The cubic nature is not completely formed at lower incident fluences,

and perfect edges are less prominent at 3.1 J/cm^2. The perfect cubic nanostructures are formed only at 3.9 J/cm^2. Upon further increase in incident fluence, the surface density of NPs appearance is reduced drastically and favors the formation of LSFL ridges as primary feature. At the fluence of 4.1 J/cm^2, the cubic-shaped particles start disappearing, and few particles are scattered at the peripheral area of the grooves and on LSFL ridges. Upon further increase in fluence, even the LSFL structures are destroyed at the fluence of 7.1 J/cm^2. The most important aspect of the effect of fluence on surface morphology is the formation of highly regular cubic-shaped copper nanoparticles. These cubic-shaped NPs are formed only at a particular fluence range when the irradiated wavelength is 860 nm. This study suggests that one can tune the formation of particle features on surfaces with incident laser parameters.

3.1.3. Laser direct writing at 900 nm

Figure 5 shows the surface morphological features of laser irradiated surfaces with the incident wavelength of 900 nm. One can see that for each fluence, the formation of LSFL is observed. As the fluence increases, the smooth LSFL are formed over a larger area. The best regular LSFL is formed at 3.5 J/cm^2 with a spatial periodicity of 662±8 nm.

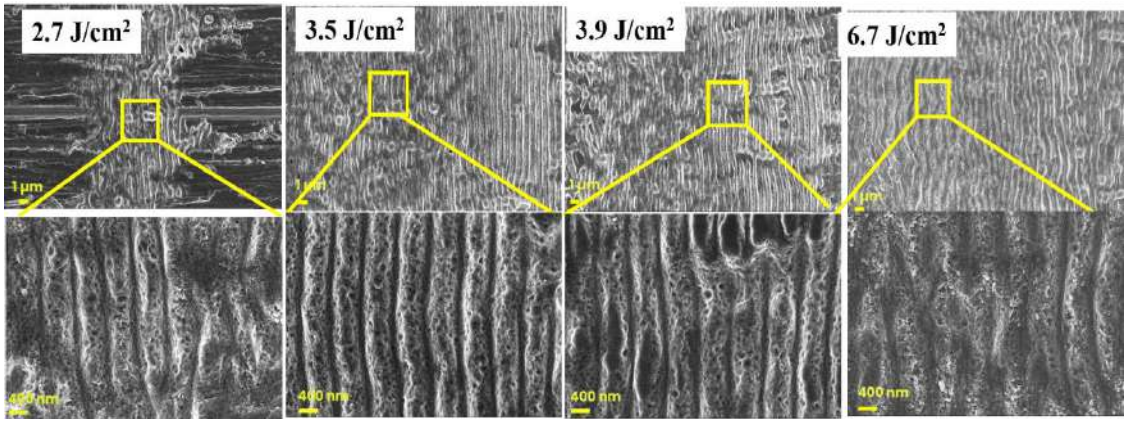

Fig 5. FESEM images of laser-induced copper surfaces for various fluence for the incident wavelength of 900 nm. The scanning speed is fixed at 0.2 mm/s. Scale bars are equal to 1 µm and 400 nm of the images in the first and second row, respectively.

There is a variation of LSFL spatial periodicity with the incident fluence on the copper irradiated surfaces, with an incident wavelength of 900 nm. The spatial periodicity increases from 632±20 nm to 693±13 nm as the fluence increases from 2.7 J/cm^2 to 5.0 J/cm^2. As we increased the fluence further, the spatial periodicity remained close to 693±13 nm. This variation of spatial periodicity with respect to fluence is shown in Fig 6. The underlying reasons behind the LIPSS formations are attributed to the interference between the surface plasmon polariton and incident laser wavelengths [40]. A rigorous analysis of wavelength-dependent LIPSS formation with the irradiation wavelength from 400-2200 nm has been reported using various optimized laser parameters [41].

3.1.4. Laser direct writing at 960 nm

The effect of incident fluence on the surface morphology is shown in Fig 7 for the incident wavelength of 960 nm. One can observe the formation of particulate-type features throughout the patterned surface for this wavelength. However,we did not observe the LIPSS formation at this wavelength, for any fluence value. For this incident wavelength, as the fluence increases, the depth of the grooves increases. At the fluence of 2.9 J/cm^2, the surface morphology at the center of the laser-focused beam looks like a molten state with several cracks throughout the grooves.

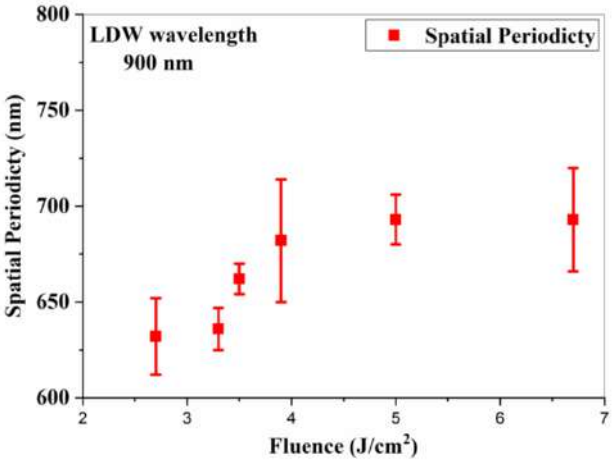

Fig 6. Variation of spatial periodicity of LSFL with incident laser fluence for the incident wavelength of 900 nm.

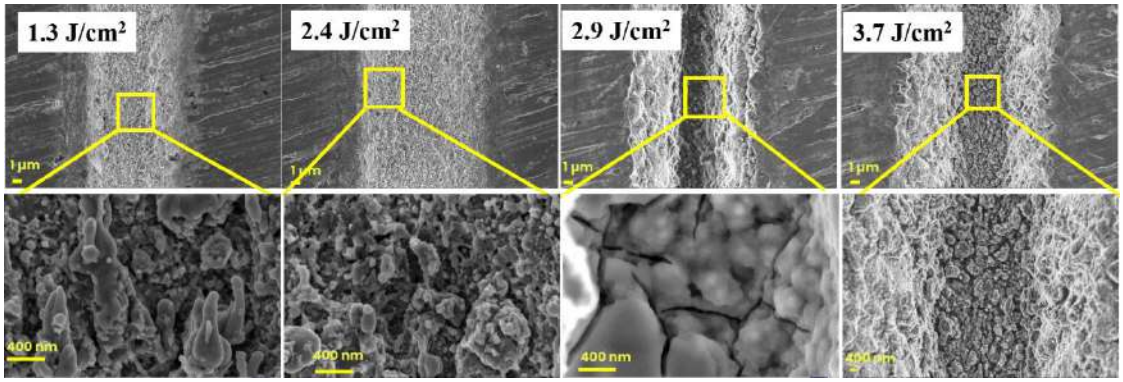

Fig 7. FESEM images of laser-induced copper surfaces for various fluences for the incident wavelength of 960 nm. The scanning speed is fixed at 0.2 mm/s. Scale bars are equal to 1 µm and 400 nm of the images in the first and second rows, respectively.

In summary, surface morphologies of laser-irradiated copper surfaces patterned with four different incident wavelengths are quite different. Each incident wavelength interacted with the surface differently and led to the formation of various surface morphologies. At the incident wavelength of 800 nm, formation of both irregular particles and LSFL are observed. In contrast, the formation of highly regular cubic-shaped NPs and LSFL appeared for the incident wavelength of 860 nm only. At the incident wavelength of 900 nm, only LSFL periodic structures formed; neither particulate-type features nor regular cubic-shaped structures are observed. Finally, at the incident wavelength of 960 nm, irregular particles are formed at the lower fluence values. The deep groove with cracks is formed at higher laser fluences.

3.1.5. Elemental analysis of different surface structures

The EDX analysis is carried out to probe the elemental composition of LIPSS, cubic features, and unpatterned surfaces. The EDX of the un-irradiated surface reveals the presence of copper only, as shown in Fig 8.

In Fig 9, the EDX is taken on two different places on the surface: (i) large area of cubic structures and (ii) small area of cubic features. It is clear from the EDX analysis, that the percentage weight of copper and oxygen is 95.51% and 4.49%, respectively, over the large area (~36 μm^2). Large area cubic features are dispersed on the copper surfaces shown in the top row of Fig 9.

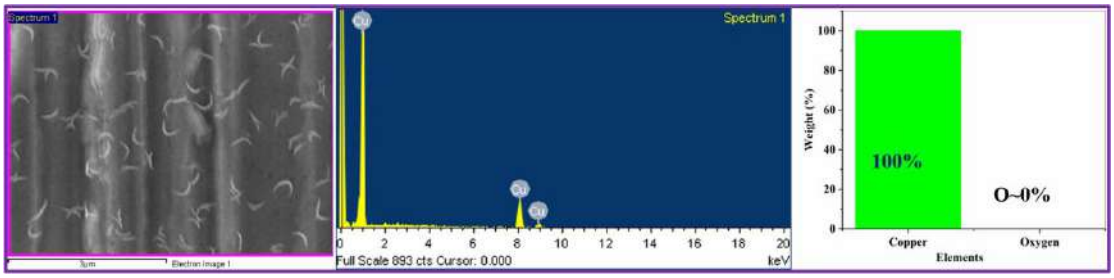

Fig 8**.** EDX analysis of the unpatterned surfaces. The scale bar is equal to 3 µm.

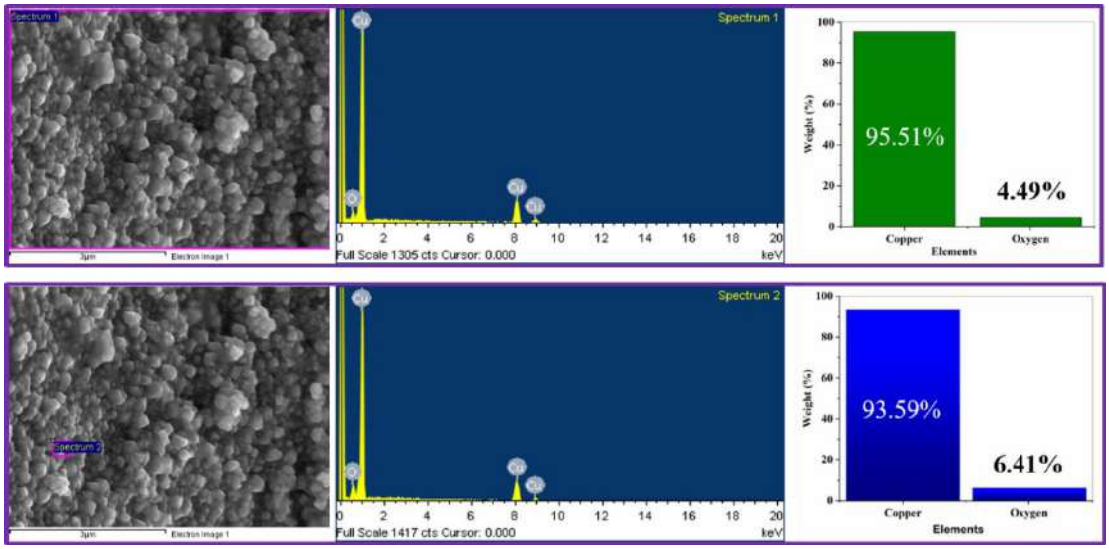

Fig 9. Energy dispersive analysis of cubic copper features. The scale bar is equal to 3 µm.

There is a slight change in elemental composition ratio when EDX is taken at a smaller area (~0.09 μm^2) close to single cube as shown in the second row of Fig 9. The presence of oxygen is found to be more on a single CuNP compared to entire region of laser-irradiated copper surface; the percentage weight of copper and oxygen are 93.59% and 6.41%, respectively. The EDX analysis depicts that oxygen is trapped on the surface during the irradiation using 860 nm, only at lower fluences. In contrast, EDX analysis depicts completely different aspects of the elemental composition of LIPSS features. The composition analysis reveals 100% copper on LIPSS surfaces with no oxygent content, Fig 10.

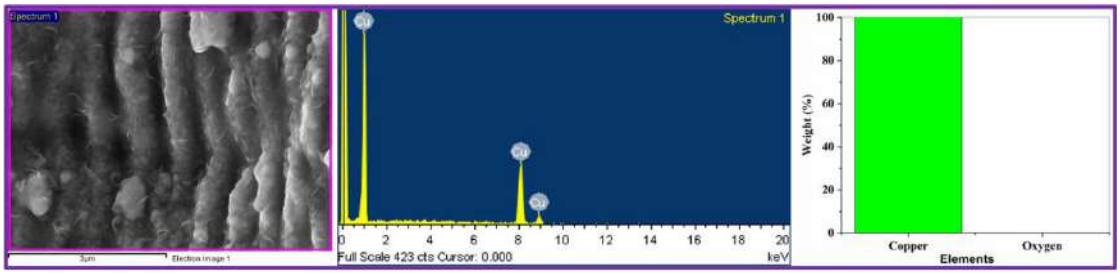

Fig 10. EDX analysis on LIPSS formation on laser-irradiated surfaces. The X-ray signatures show it is pure copper, and the result is the same all over the surface. The scale bar is equal to 3 µm.

In summary, the compositions of LIPSS are purely periodic modulation of copper materials itself, whereas cubic features are composites of copper and oxygen elements. Further studies and experiments are needed to understand the underlying physics, and the reason why the oxygen being trapped during the irradiation of 860 nm only but not at other wavelengths.

4 Conclusions

Controlled fabrication of cubic-shaped copper NPs on the surface of copper is shown for the first time. This can be achieved uniquely via femtosecond laser irradiation using a particular incident wavelength, scanning speed, and incident laser fluence. The study shows that the surface topological structures could be controlled or varied using different wavelengths and irradiation energies. The ideal wavelength for the formation of LIPSS over a broad range of energies is 900 nm. The variation of the LIPSS periodicity with energy is presented for 900 nm; at higher fluences, the periodicities remain constant until they get randomized at destruction energies. At 960 nm of irradiation wavelength, we could not observe any LIPSS formation for any incident energy. Cubic-shaped nanoparticles will have more effective surface area due to their edges, and they have a wide range of potential applications, particularly as electrodes in catalytic reactions. The formation of the cubic structures is due to the trapping of oxygen; this process is favored only at the 860 nm central wavelength of femtosecond pulses. We believe this type of wavelength-dependent surface structuring will have many more potential applications and new physics to be explored in many more materials.

Acknowledgments

The financial support from DST-SERB (EMR/000516), DST-Purse, Respond Project ISRO, and UoH Institute of Eminence (IoE) grant- RC1-20-011. Md Abu Taher acknowledges a fellowship from UGC-MANF, India, for financial support.

References

1. Chan G H, Zhao J, Hicks E M, Schatz G C, Duyne R P, Plasmonic properties of copper nanoparticles fabricated by nanosphere lithography, *Nano Lett*, 7(2007)1947–1952.
2. Radi A, Pradhan D, Sohn Y, Leung K T, Nanoscale Shape and Size Control of, *ACS Nano*, 4(2010)1553–1560.
3. Gawande M B, Goswami A, Felpin F X, Asefa T, Huang X, Silva R, Zou X, Zboril R, Varma R S, Cu and Cu-Based Nanoparticles: Synthesis and Applications in Catalysis, *Chem Rev*, 116(2016)3722–3811.
4. Lohrasbi S, Sheikholeslami M, Ganji D D, Multi-objective RSM optimization of fin assisted latent heat thermal energy storage system based on solidification process of phase change Material in presence of copper nanoparticles, *Appl Therm Eng*, 118(2017)430–447.
5. Tamilvanan A, Balamurugan K, Ponappa K, Kumar B M, Copper nanoparticles: Synthetic strategies, properties and multifunctional application, *Int J Nanosci*, 13(2014); doi.org/10.1142/S0219581X14300016.
6. Shin D, Banerjee D, Enhancement of specific heat capacity of high-temperature silica-nanofluids synthesized in alkali chloride salt eutectics for solar thermal-energy storage applications, *Int J Heat Mass Transf*, 54(2011) 1064–1070.
7. Deka P, Borah B J, Saikia H, Bharali P, Cu-Based Nanoparticles as Emerging Environmental Catalysts, *Chem Rec*, 19(2019)462–473.
8. Saran S, Manjari G, Devipriya S P, Synergistic eminently active catalytic and recyclable Ag, Cu and Ag-Cu alloy nanoparticles supported on TiO_2 for sustainable and cleaner environmental applications: A phytogenic mediated synthesis, *J Clean Prod*, 177(2018)134–143.
9. Tang S C N, Lo I M C, Magnetic nanoparticles: Essential factors for sustainable environmental applications, *Water Res*, 47(2013)2613–2632.
10. Abdelbasir S M, McCourt K M, Lee C M, Vanegas D C, Waste-Derived Nanoparticles: Synthesis Approaches, Environmental Applications, and Sustainability Considerations, *Front Chem*, 8(2020)782; doi.org/10.3389/fchem.2020.00782.

11. Din M I, Rehan R, Synthesis, Characterization, and Applications of Copper Nanoparticles, *Anal Lett*, 50(2017) 50–62.
12. Tauran Y, Brioude A, Coleman A W, Rhimi M, Kim B, Molecular recognition by gold, silver and copper nanoparticles, *World J Biol Chem*, 4(2013)35; doi.org/10.4331/wjbc.v4.i3.35.
13. Muniz-Miranda M, Gellini C, Giorgetti E, Surface-enhanced Raman scattering from copper nanoparticles obtained by laser ablation, *J Phys Chem C*, 115(2011)5021–5027.
14. Baruah P K, Singh A, Rangan L, Sharma A K, Khare A, Optimization of copper nanoparticles synthesized by pulsed laser ablation in distilled water as a viable SERS substrate for karanjin, *Mater. Chem. Phys*, 220(2018)111–117.
15. Zhang X, Xu S, Jiang S, Wang J, Wei J, Xu S, Gao S, Liu H, Qiu H, Li Z, Liu H, Li Z, Li H, Growth graphene on silver-copper nanoparticles by chemical vapor deposition for high-performance surface-enhanced Raman scattering, *Appl Surf Sci*, 353(2015)63–70.
16. Fang H, Wen M, Chen H, Wu Q, Li W, Graphene stabilized ultra-small CuNi nanocomposite with high activity and recyclability toward catalysing the reduction of aromatic nitro-compounds, *Nanoscale*, 8(2016)536–542.
17. Wang Y, Duan X, Xie Y, Sun H, Wang S, Nanocarbon-Based Catalytic Ozonation for Aqueous Oxidation: Engineering Defects for Active Sites and Tunable Reaction Pathways, *ACS Catal*, 10(2020)13383–13414.
18. Swarnkar R K, Singh S C, Gopal R, Effect of aging on copper nanoparticles synthesized by pulsed laser ablation in water: Structural and optical characterizations, *Bull Mater Sci*, 34(2011)1363–1369.
19. Hudson R, Feng Y, Varma R S, Moores A, Bare magnetic nanoparticles: Sustainable synthesis and applications in catalytic organic transformations, *Green Chem*, 16(2014)4493–4505.
20. Karimi B, Mansouri F, Mirzaei H M, Recent Applications of Magnetically Recoverable Nanocatalysts in C-C and C-X Coupling Reactions, *ChemCatChem*, 7(2015)1736–1789.
21. Liu P, Wang H, Li X, Rui M, Zeng H, Localized surface plasmon resonance of Cu nanoparticles by laser ablation in liquid media, *RSC Adv*, 5(2015)79738–79745.
22. Wei C, Liu Q, Shape-, size-, and density-tunable synthesis and optical properties of copper nanoparticles, *CrystEngComm*, 19(2017)3254–3262.
23. Sadrolhosseini A R, Noor A S B M, Shameli K, Mamdoohi G, Moksin M M, Mahdi M A, Laser ablation synthesis and optical properties of copper nanoparticles, *J Mater Res*, 28(2013)2629–2636.
24. Haq I U, Akhtar K, Malook K, Synthesis and characterization of monodispersed copper oxide and their precursor powder, *Mater Res Bull*, 57(2014)121–126.
25. Zizzo J, Toxicity effects of Cubic Cu_2O nanoparticles on defecation rate and length in C Elegans, *Biomed Res Ther*, 7(2020)4045–4051.
26. Tan M I S M H, Omar A F, Rashid M, U. Hashim U, VIS-NIR spectral and particles distribution of Au, Ag, Cu, Al and Ni nanoparticles synthesized in distilled water using laser ablation, *Results Phys*, 14(2019)102497; doi.org/10.1016/j.rinp.2019.102497.
27. Ngo C V, Chun D M, Control of laser-ablated aluminum surface wettability to superhydrophobic or superhydrophilic through simple heat treatment or water boiling post-processing, *Appl Surf Sci*, 435(2018)974–982.
28. Martínez-Calderon M, Rodríguez A, Dias-Ponte A, Morant-Miñana M C, Gómez-Aranzadi M, Olaizola S M, Femtosecond laser fabrication of highly hydrophobic stainless steel surface with hierarchical structures fabricated by combining ordered microstructures and LIPSS, *Appl Surf Sci*, 374(2016)81–89.
29. Taher M A, Prasad H, Krishnan P K N, Desai N R, Naraharisetty S R G, Ellipsoidal droplet formation on anisotropic superhydrophobic copper surface, *Surf Topogr Metrol Prop*, 7(2019); doi.org/10.1088/2051-672X/ab2d80.
30. Taher M A, Prasad H, Krishnan P K N, Desai N R, Naraharisetty S R G, The validity of triple contact line theory from hydrophilic to superhydrophobic surfaces, *J Phys D Appl Phys*, 55(2022)055305; doi.org/10.1088/1361-6463/ac30b8.
31. Müller F A, Kunz C, Gräf S, Bio-inspired functional surfaces based on laser-induced periodic surface structures, *Materials* (*Basel*), 9(2016); doi.org/10.3390/ma9060476.
32. Taher M A, Ponnan S, Prasad H, Rao D N, Naraharisetty S R G, Broadband absorption of nanostructured stainless steel surface fabricated by nanosecond laser irradiation, *Nanotechnology*. 31(2020)175301; doi.org/10.1088/1361-6528/ab674e.

33. Taher M A, Naraharisetty S R G, Rao D N, Super black stainless steel surface fabricated by nanosecond laser irradiation, *Opt InfoBase Conf Paper*. Part F181- (2020); doi.org/10.1364/CLEO_AT.2020.JW2B.21.
34. Zhang X, Shi F, Niu J, Jiang Y, Wang Z, Superhydrophobic surfaces: From structural control to functional application, *J Mater Chem*, 18(2008)621–633.
35. Roy N K, Dibua O G, Jou W, He F, Jeong J, Wang Y, Cullinan M A, A comprehensive study of the sintering of copper nanoparticles using femtosecond, nanosecond, and continuous wave lasers, *J. Micro Nano-Manufacturing*. 6(2018)1–21.
36. Sadrolhosseini A R, Rashid S A, Zakaria A, Shameli K, Green fabrication of copper nanoparticles dispersed in walnut oil using laser ablation technique, *J Nanomater*, 2016(2016); doi.org/10.1155/2016/8069685.
37. Harishchandra B D, Pappuswamy M, PU A, Shama G, Pragatheesh A, Arumugam V A, Periyaswamy T, Sundaram R, Copper Nanoparticles: A Review on Synthesis, Characterization and Applications, *Asian Pacific J Cancer Biol,* 5(2020)201– 210.
38. Khodashenas B, Ghorbani H R, Synthesis of copper nanoparticles: An overview of the various methods, *Korean J Chem Eng*. 31(2014)1105–1109.
39. Goncharova D A, Kharlamova T S, Lapin I N, Svetlichnyi V A, Chemical and Morphological Evolution of Copper Nanoparticles Obtained by Pulsed Laser Ablation in Liquid, *J Phys Chem C*. 123(2019)21731–21742.
40. Bonse J, Gräf S, Maxwell Meets Marangoni—A Review of Theories on Laser-Induced Periodic Surface Structures, *Laser Photonics Rev*, 14(2020)1–25.
41. Taher M A, Chaudhary N, Thirunaukkarasu K, Rajput V K, Naraharisetty S R G, Controlled periodicities of ladder-like structures via femtosecond laser of wavelength from 400 nm to 2200 nm, *Surf Interfaces*, 28(2022)101622; doi.org/10.1016/j.surfin.2021.101622.

[*Received*: 01.08.2021; r*evised recd*: 15.09.2021; *accepted*: 01.10.2021]